The diversity in thermal behavior of novel catanionic cholates: the dominant effect of quaternary ammonium centers

Tea Mihelj[a,*], Danijela Vojta[b], Vlasta Tomašić[a]

[a]*Department of Physical Chemistry*, [b]*Department of Organic Chemistry and Biochemistry*,

Ruđer Bošković Institute, POB 180, HR-10002 Zagreb, Croatia

***Corresponding Author:** Tea Mihelj

Laboratory for synthesis and processes of self-assembling of organic molecules

Department of Physical Chemistry, Ruđer Bošković Institute

Bijenička c. 54, P.O.Box 180, HR–10002 Zagreb, CROATIA

E-mail: tmihelj@irb.hr

FAX: +385 1 4680 245

TEL: +385 1 4571 211

ABSTRACT

The thermal behavior of novel catanionic compounds based on cholate anion was examined. The study explains the effect of the raising dodecyl chain number, as well as of the raising headgroup number in quaternary ammonium salts on their physico-chemical properties. The examined samples are crystal smectic phases at room temperature. Their rich and diverse thermal behavior is seen through polymorphic phase transitions, thermotropic mesomorphism of smectic nature and in some cases, kinetically managed crystallization that lasts in days. The changes of the cholates keto-enol isomer balance during thermal treatment are obtained. For both groups of samples temperatures of isotropisation and the thermodynamic parameters follow polynomial regression. Introduction of the new dodecyl chain leads to more ordered structure, while implementation the new headgroup leads to advanced polymer-like structure. The obtained results demonstrate an effort for getting and controlling the regularity of the physico-chemical and thermotropic properties for new compounds by systematic changing of cationic part of the molecule. These informations could provide in the future the easiest way for selection of potentially new and targeted applicable materials.

Keywords: cholate anion, infrared spectroscopy, nuclear magnetic resonance spectroscopy, smectic, thermotropic behavior

1. Introduction

Molecular self-assembly is a process in which molecules spontaneously organize into ordered assemblies, such as biomembranes, multimeric proteins and nucleic acid multiplexes [1], by noncovalent intermolecular forces. Inspired by these biological architectures, the design of molecular-recognition complexes, liquid crystals and solid state structures has been an active field of chemistry. Supramolecular hybrid membranes can be easily synthesized when using amphiphiles as constituents [2,3], mostly due to the same nature and behavior as of phospholipids that build biomembranes and living cells andnowadays, varied morphologies such as vesicles and lamellas, as well as tubes, disks and helices are available from synthetic amphiphiles [4–8]. The structures and properties of resulted aggregates in solution or in solid state can be controlled by tuning the chemical structure of the constituent amphiphiles.

Cholic acid is anionic steroidal biosurfactant classified as a natural bile acid, very often used in different pharmacological applications [9–12], and as building block in supramolecular chemistry [13–16]. Regarding the latter, some cholic acid based macrocycles like cholaphanes are used as transmembrane anion carriers [17], cyclocholates in host-guest chemistry or molecular recognition studies [18], and bile acid based chiral dendrons [19], or molecular boxes [20] in nanotechnology. It is already known that cholic acid forms inclusion crystals with various guest compounds. Diversity is the result of the hierarchical structure in steroids, based on characteristic bimolecular and helical 2_1 screw assemblies[21],where facial amphiphilicity of molecules[22], type of guest components[23], and various combination of hydrogen-bonding arrangements, play exceptionally important role.

Molecular crystals of surfactant molecules differ from other classes of solids in being made up of discrete molecules ordered threedimensionally, and the structure is influenced by both strong and weaker intramolecular forces. The thermal behavior of solid amphiphiles depends on the molecular packing properties, which include lenght, branching and unasaturation of hydrocarbon chain, polar headgroup and the counterion size [24]. The consequence of weak intramolecular forces are, in much easier way, induced molecular motions by the temperature, causing transformations into new phases of which one can be the liquid crystal. Formation of such structures are very often seen for quartenary ammonium salts [4,25–27], that promote mesomorphic properties of the catanionic systems. Thermotropic mesomorphism of catanionic molecules is mostly of the smectic (Sm) nature, with the molecules organized in layers, possessing positional, conformational and orientational order, and resembling, again, the biomembranes [5,27–31]. Unlike for previous examples, alkylammonium picrates are of high crystallinity, and form blade textures without mesomorphic properties, but with bilayer-like arrangement [4,27,32]. Host-guest compounds of cholic acid with *n*-alkylammonia reveal two types of bilayer-like structures; 1:1 complexes build a kind of sandwich-type structure, while in

2:1 compound bilayers cross and form one-dimensional hydrophobic channels into which guest molecules are included [23]. As the consequence of specific structural behavior, alkylammonium cholates differ in their thermal properties. Dioctyldimethylammonium and dinonyldimethylammonium cholates are characterized as polymorphs, but without mesophase formation [33]. Dodecylpyridinium cholate is crystal smectic at room temperature, with fully extended and tilted catanionic molecule, which goes through melting and partial degradation, ending with total decomposition and carbonization when heated [27]. However, poly(oxyethylene) cholesterol ethers with short oxyethylene chains exhibit liquid crystal appearance with antiparalel or zigzag packing in the layers, related to the predominance of the steroidal part. For long oxyethylene chains, the polymer gains in importance and only polymorphism is observed at low temperatures [34].

Complexes formed by cholic acid or sodium cholate, capable of forming hybrid membranes and imitating their structure and function, are rarely examined in terms of their thermal properties. Depending on the structural parameters these complexes are rather thermally stable and might possess mesomorphic properties. Therefore, it was interesting to synthesize new catanionic compounds based on cholate anion with different quaternary ammonium part that could induce or enhance thermotropic properties of mentioned catanionics. The quaternary ammonium salts chosen in this study differ either in the alkyl chain number on the same headgroup, or in the number of headgroups. This article represents an attempt to explain the effect of the diversity in thermal behavior and the conditions for mesophase formation of novel catanionic cholates, depending on varied alkyl chain and headgroup numbers. The main goal of this study is to carry out the complete thermal characterization of synthesized compounds through several complementary techniques (thermogravimetric, differential thermal analysis, optical microscopy, differential scanning calorimetry, and temperature-dependent infrared spectroscopy) and to present defined regularities that connect structural and physico-chemical properties.

2. Experimental

2.1. Materials

Sodium cholate hydrate, *i.e.* 3α,7α,12α-trihydroxy-5β-cholanic-acid sodium salt ($C_{24}H_{39}O_5Na$, M_w/ g mol^{-1}= 430.60; Sigma Ultra, min. 99%) was obtained from Sigma Aldrich. Quaternary ammonium salts: dodecyltrimethylammonium bromide ($C_{15}H_{34}NBr$, M_w/ g mol^{-1}= 308.35, puriss. p.a. > 99.0 %) and tridodecylmethylammonium chloride ($C_{37}H_{78}NCl$, M_w/ g mol^{-1}= 572.49, puriss. p.a. ≥ 97.0 %) were obtained from Fluka, while didodecyldimethylammonium bromide ($C_{26}H_{56}NBr$, M_w/ g mol^{-1}= 462.64, puriss p.a. > 99.0 %) from Acros Organics. Chemicals were used without further purification. Dimeric and oligomeric surfactant bromides used for this study possess the same spacer group separating the unimeric units. They were synthesized in our laboratory [25]: (12–2–12), 2Br *i.e.* bis(*N*,*N*-dimethyl-*n*-dodecyl)ethylene-1,2-diammonium dibromide; (12–2–12–2–12), 3Br *i.e.N*-bis[2-(*N'*,*N'*-dimethyl-*n*-dodecylammonio)ethylene]-*n*-dodecyl-*N*-methyl-1,2-diammonium tribromide; and (12–2–12–2–12–2–12), 4Br *i.e.* *N*,*N'*-bis[2'-(*N''*,*N''*-dimethyl-*n*-dodecylammonio)ethylene]-di-*n*-dodecyl-*N*,*N'*-dimethyl-ethylene-1,2-diammonium tetrabromide.

2.2. Synthesis of catanionic surfactants

Catanionic cholates **1**, **2**, and **4**-**6** were synthesized by mixing heated equimolar aqueous solutions of quaternary ammonium bromide and sodium cholate. The exception was compound **3** that was synthesized from ethanol due to the low solubility of tridodecylmethylammonium chloride in water, so cholic acid (high solubility in ethanol) was also used for this purpose. After the preparation, systems were thermostated at *T*/ K= 293 and aged. Samples were filtrated after 5-7 days of aging, washed with water to remove co-precipitated electrolyte, dried under vacuum for 24 h, and stored protected from moisture and light before use. Compounds **1**, **2**, **4** and **5** precipitated as white powder, while compounds **3** and **6** were gelatin-like, elastic mass. Scheme 1. shows the synthesized catanionic compounds as follows: dodecyltrimethylammonium cholate (abbreviated as compound **1**); didodecyldimethylammonium cholate (**2**); tridodecylmethylammonium cholate (**3**); bis(*N*,*N*-dimethyl-*n*-dodecyl)ethylene-1,2-diammonium dicholate (**4**); *N*-bis[2-(*N'*,*N'*-dimethyl-*n*-dodecylammonio)ethylene]-*n*-dodecyl-*N*-methyl-1,2-diammonium tricholate (**5**); *N*,*N'*-bis[2'-(*N''*,*N''*-dimethyl-*n*-dodecylammonio)ethylene]-di-*n*-dodecyl-*N*,*N'*-dimethyl-ethylene-1,2 diammonium tetracholate,(**6**).

Scheme 1. The structure of examined quaternary ammonium cholates: dodecyltrimethylammonium cholate (**1**); didodecyldimethylammonium cholate (**2**); tridodecylmethylammonium cholate (**3**);

bis(*N*,*N*-dimethyl-*n*-dodecyl)ethylene-1,2-diammonium dicholate (**4**); *N*-bis[2-(*N'*,*N'*-dimethyl-*n*-dodecylammonio)ethylene]-*n*-dodecyl-*N*-methyl-1,2-diammonium tricholate (**5**); *N*,*N'*-bis[2'-(*N''*,*N''*-dimethyl-*n*-dodecylammonio)ethylene]-di-*n*-dodecyl-*N*,*N'*-dimethyl-ethylene-1,2 diammonium tetracholate(**6**).

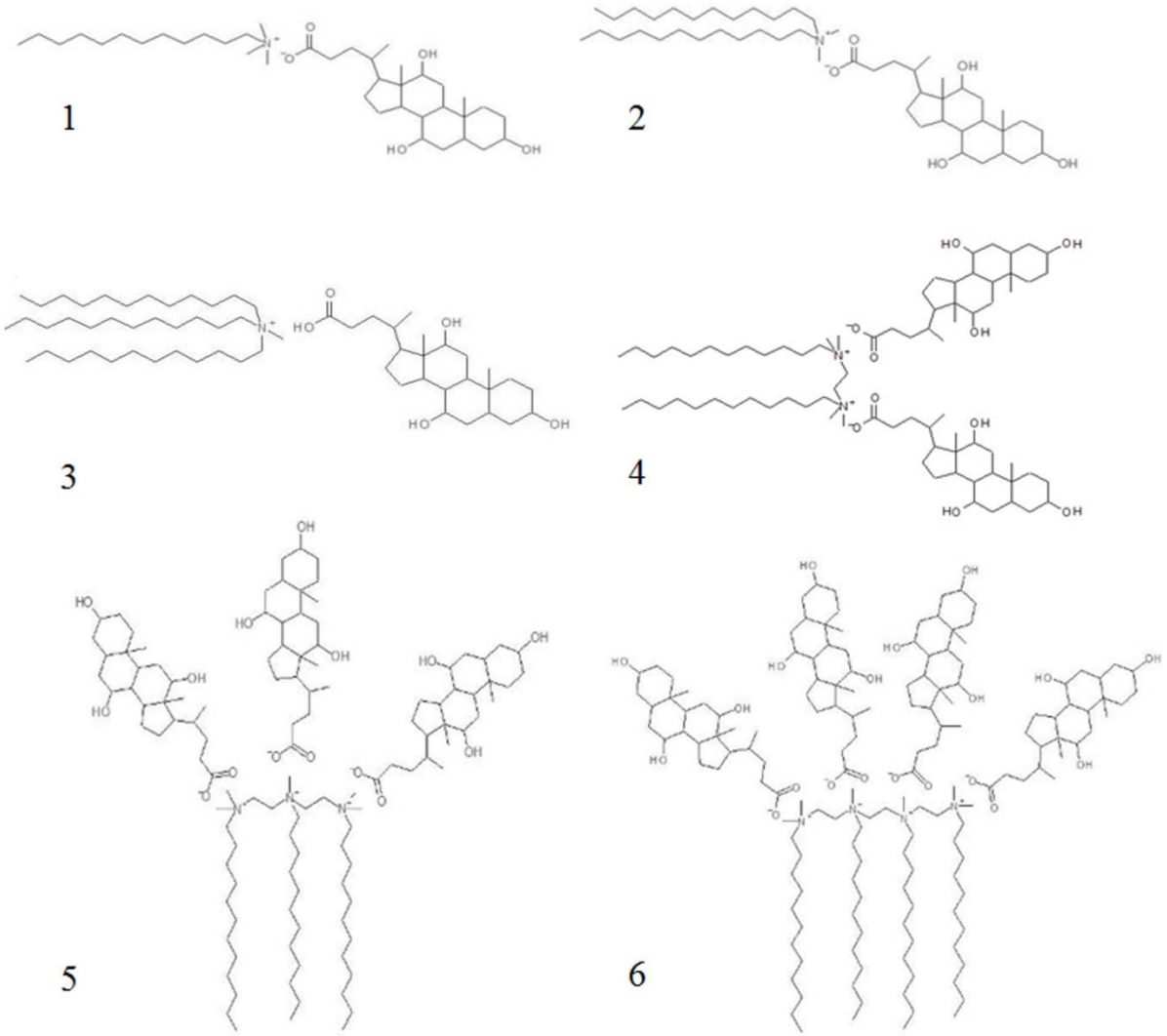

The identification and purity check was performed by *nuclear magnetic resonance spectroscopy*, NMR (Avance 600 Bruker with supraconducting magnet, 14 T field strength, and frequency range 24-600 MHz) according to the following designation: Compounds **1-3**

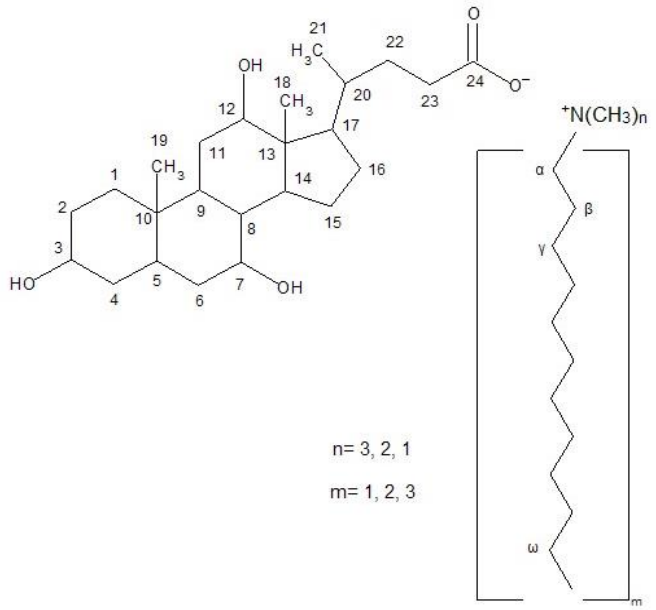

Compound 1(M_w/ g mol^{-1}= 636.02).^{13}C NMR (150 MHz, DMSO-d_6) σ/ppm: 175.68 (C24), 71.04 (C12), 70.38 (C3), 66.24 (C7), 65.18 (α-$CH_{2\ dodecyl}$), 52.04 (CH_3N), 46.58 (C17), 45.70 (C13), 41.58 (C5), 41.24 (C14), 39.53 (C8), 39.37 (C4), 36.41 (C1), 35.76 (C20), 35.35 (C23), 34.89 (C10), 34.35 (C6), 33.13 (C22), 31.24 (β-$CH_{2\ dodecyl}$), 30.36 (C2), 29.03- 28.42 (γ-$CH_{2dodecyl}$, $(CH_2)_6$), 27.39 (C16), 26.07 (C9), 25.75 (CH_2), 22.85 (C15), 22.52 (C19), 22.07- 21.98 (2 CH_2), 17.33 (C21), 13.88 (ω- CH_3), 12.39 (C18).^{1}H NMR (600 MHz, DMSO-d_6) σ/ppm; 4.31 (1H, s br, OH-C3), 4.08 (1H, s br, OH-C12), 3.99 (1H, s br, OH-C7), 3.78 (1H, s, C12), 3.60 (1H, s, C7), 3.28- 3.24 (2H, m, α-$CH_{2\ dodecyl}$), 3.20- 3.14 (1H, m, C3), 3.03 (9H, s, CH_3N), 2.26-2.18 (1H, q, *J*=12.96, C4α), 2.18- 2.12 (1H, dt, *J*= 4.6, 5.074, C9), 2.00- 1.93 (1H, dt, *J*=7.40, 4.62,C14), 1.83- 1.68 (5H, m, C23, C1α, C17, C16α), 1.68- 1.53 (5H, m, C15β, C6β, β-$CH_{2\ dodecyl}$, C22α), 1.47-1.38 (4H, m, C4β, C2β, C11), 1.38-1.13 (24H, m, C6α, C8, C2α, γ-CH_2, $(CH_2)_{8\ dodecyl}$, C20, C5, C16β), 1.06-0.99 (1H, m, C22β), 0.97-0.89 (1H, m, C15α), 0.87 (3H, d, *J*=6.6, C21), 0.85 (3H, t, *J*=7.1, ω- $CH_{3\ dodecyl}$), 0.83 (1H, m, partly under ω-$CH_{3\ dodecyl}$ peak, C1β), 0.80 (3H, s, C19), 0.57 (3H, s, C18).

Compound 2(M_w/ g mol^{-1}= 790.30).^{13}C NMR (150 MHz, DMSO-d_6) σ/ppm: 175.39 (C24), 71.04 (C12), 70.38 (C3), 66.24 (C7), 62.79 (α-$CH_{2\ dodecyl}$), 49.95 (CH_3N), 46.53 (C17), 45.69 (C13), 41.52 (C5), 41.26 (C14), 39.50 (C8), 39.37 (C4), 36.36 (C1), 35.70 (C20), 35.30 (C23), 34.82 (C10), 34.35 (C6), 33.13 (C22), 31.20 (β-$CH_{2\ dodecyl}$), 30.35 (C2), 28.94- 28.57 (γ-$CH_{2dodecyl}$, $(CH_2)_6$), 28.35(CH_2), 28.48 (C11), 27.34(C16), 26.12 (C9), 25.65 (CH_2), 22.81 (C15), 22.52 (C19), 21.99 (CH_2), 21.57 (CH_2), 17.34 (C21), 13.83 (ω- CH_3), 12.37 (C18).^{1}H NMR (600 MHz, DMSO-d_6) σ/ppm; 4.30 (1H, s br, OH-C3), 4.07 (1H, s br, OH-C12), 3.98 (1H, s br, OH-C7), 3.78 (1H, s, C12), 3.61 (1H, s, C7), 3.24- 3.14 (5H, m, α-$CH_{2\ dodecyl}$, C3), 2.98 (6H, s, CH_3N), 2.26-2.19 (1H, q, *J*=13.04, C4α),2.19- 2.12 (1H, dt, *J*=4.60, 4.96, C9), 2.00- 1.93 (1H, dt, *J*=7.48, 4.72,C14), 1.84- 1.68 (5H, m, C23, C1α, C17, C16α), 1.67- 1.55 (5H, m, C15β, C6β, β-$CH_{2\ dodecyl}$, C22α), 1.47-1.38 (4H, m, C4β, C2β, C11), 1.38- 1.13 (46H, m, C6α, C8, C2α, γ-CH_2, $(CH_2)_{8\ dodecyl}$, C20, C5, C16β), 1.07-1.00 (1H, m, C22β), 0.97- 0.89 (1H, m, C15α), 0.89 (3H, d, *J*=6.5, C21), 0.86 (6H, t, *J*=7.1, ω- $CH_{3\ dodecyl}$), 0.83 (1H, m, partly under ω-$CH_{3\ dodecyl}$ peak, C1β), 0.80 (3H, s, C19), 0.57 (3H, s, C18).

Compound 3(M_w/ g mol^{-1}= 944.60).^{13}C NMR (150 MHz, DMSO-d_6) σ/ppm: 174.94 (C24), 70.95 (C12), 70.38 (C3), 66.19 (C7), 60.43 ((α-CH_2), 47.49 (NCH_3), 46.04 (C17), 45.71 (C13), 41.48 (C5), 41.31 (C14), 39.44 (C8), 39.36 (C4), 35.26 (C1), 34.98 (C20), 34.82 (C23), 34.33 (C10), 31.24 (β-$CH_{2\ dodecyl}$), 30.90 (C22), 30.78 (C6), 30.35 (C2), 28.97 (γ-$CH_{2\ dodecyl}$), 28.85, 28.65, 28.30 (($CH_2)_6$),

28.47 (C11), 27.20 (C16), 26.16 (C9), 25.66 (CH_2), 22.73 (C15), 22.56 (C19), 22.01 (CH_2), 21.21 (CH_2), 16.89 (C21), 13.85 (ω- CH_3), 12.27 (C18).^{1}H NMR (600 MHz, DMSO-d_6) σ/ppm; 4.29 (1H, s br, OH-C3), 4.09 (1H, s br, OH-C12), 4.00 (1H, s br, OH-C7), 3.78 (1H, s, C12), 3.61 (1H, s, C7), 3.45- 3.42 (1H, m, *J*= 6.95, C3), 3.22-3.14 (6H, m, α-$CH_{2\ dodecyl}$), 2.93 (3H, s, CH_3-N), 2.24-2.06 (4H, m, C4α, C23α, C9, C23β), 2.00- 1.95 (1H, dt, *J*=7.64, 4.63,C14), 1.81- 1.68 (3H, m, C17, C16α, C6β), 1.68- 1.58 (9H, m, β-$CH_{2\ dodecyl}$, C1α, C22α, C15β), 1.47- 1.40 (4H, m, C4β, C2β, C11α, C11β), 1.40- 1.13 (61H, m, C6α, C8, C2α, γ-CH_2, C20, $(CH_2)_{8\ dodecyl}$, C5, C22β, C16β), 1.06- 1.04 (1H, m, C1β), 0.99- 0.93 (1H, m, C15α), 0.91 (3H, d, *J*=6.5, C21), 0.86- 0.84 (9H, t, *J*=7.1, ω- $CH_{3\ dodecyl}$), 0.80 (3H, s, C19), 0.58 (3H, s, C18).

Compounds **4-6**

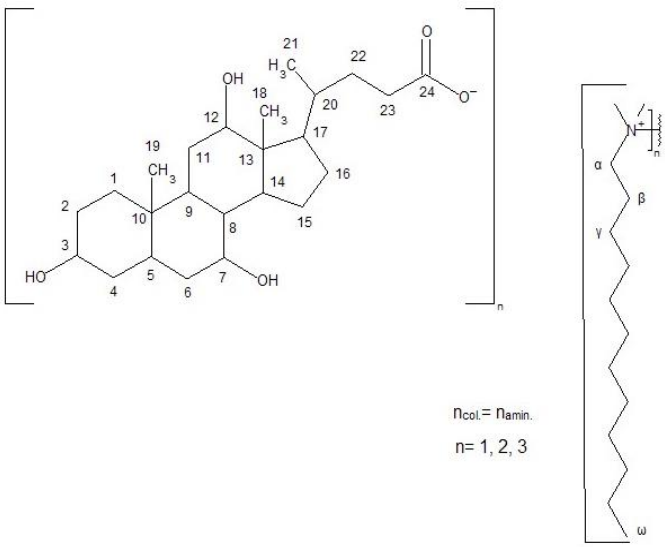

Compound 4(M_w/ g mol^{-1}= 1270.01).^{13}C NMR (150 MHz, DMSO-d_6, 323K) σ/ppm: 70.88 (C12), 70.17 (C3), 66.08 (C7), 64.35 (α-$CH_{2\ dodecyl}$), 55.16 (NCH_2CH_2N) 50.03 (CH_3N), 46.31 (C17), 45.53 (C13), 41.30 (C5), 41.97 (C14), 39.64 (C8), 39.30 (C4), 35.11 (C20), 34.98 (C23), 34.51 (C10), 34.04 (C6), 30.73 (C22), 30.08 (β-$CH_{2\ dodecyl}$), 28.49- 28.12 (γ-$CH_{2dodecyl}$, $(CH_2)_5$), 28.43 (C2), 28.10 (C11),28.00 (CH_2), 26.80 (C16), 25.96 (C9), 25.39 (CH_2), 22.42 (C15), 22.13 (C19), 21.41 (CH_2), 17.05 (C21), 13.22 (ω- CH_3), 12.02 (C18).^{1}H NMR (600 MHz, DMSO-d_6, 50 °C) σ/ppm; 3.97 (2H, s, OH-C12), 3.92 (2H, s br, OH-C7), 3.80 (4H, m, NCH_2CH_2N), 3.65 (2H, s, C12), 3.59 (2H, s br, C7), 3.41- 3.36 (4H, m, α-$CH_{2\ dodecyl}$), 3.24- 3.19 (2H, m, C3), 3.02 (12H, s, CH_3N), 2.27-2.16 (4H, m, C4α, C9),2.03- 1.97 (2H, dt, *J*=7.4, 4.6,C14), 1.89- 1.79 (10H, m, C23, C1α, C17, C16α), 1.78- 1.60 (10H, m, C15β, C6β, β-$CH_{2\ dodecyl}$, C22α), 1.51-1.43 (8H, m, C4β, C2β, C11), 1.43- 1.18 (48H, m, C6α, C8, C2α, γ-CH_2, $(CH_2)_{8\ dodecyl}$, C20, C5, C16β), 1.16-1.09 (2H, m, C22β), 1.01- 0.93 (2H, m, C15α), 0.91 (6H, d, *J*=6.5, C21), 0.87 (6H, t, *J*=7.1, ω- $CH_{3\ dodecyl}$), 0.83 (2H, m, partly under ω-$CH_{3\ dodecyl}$ peak, C1β), 0.83 (9H, s, C19), 0.61 (6H, s, C18).

Compound 5(M_w/ g mol^{-1}= 1903.99).^{13}C NMR (150 MHz, DMSO-d_6, 323 K) σ/ppm: 175.94 (C24), 71.06 (C12), 70.26 (C3), 66.18 (C7), 63.71 (α-$CH_{2\ dodecyl}$), 59.88 (NCH_2CH_2N) 49.99 (CH_3N), 49.93 (NCH_2CH_2N), 46.47 (C17), 45.61 (C13), 41.47 (C5), 41.10 (C14), 39.46 (C8), 39.37 (C4), 36.15 (C1), 35.56 (C20), 35.23 (C23), 34.79 (C10), 34.24 (C6), 31.07 (CH_2), 32.94 (C22), 30.24 (C2),28.69- 28.86 ($(CH_2)_4$), 28.27- 28.50 ($(CH_2)_3$), 27.18(C11), 26.02 (C9), 25.75 (C16), 25.66 (CH_2), 22.70 (C15), 22.32 (C19), 21.82 (γ-$CH_{2\ dodecyll}$), 21.72 (β-$CH_{2\ dodecy}$), 22.01 (CH_2), 21.21 (CH_2), 17.22

(C21), 13.60 (ω- CH_3), 12.24 (C18).^{1}H NMR (600 MHz, DMSO-d_6, 50 °C) σ/ppm; 4.21 (3H, s br, OH-C3), 3.98 (3H, s br, OH-C12), 3.89 (3H, s br, OH-C7), 3.79 (3H, s, C12), 3.62 (3H, s, C7), 3.49-3.46 (4H, t, *J*=6.56, NCH_2CH_2N), 3.34- 3.31 (6H, m, α-$CH_{2\ dodecyl}$), 3.20 (3H, under water, C3), 3.08 (15H, s, CH_3-N), 2.86- 2.83 (4H, t, *J*=6.56, NCH_2CH_2N), 2.26-2.15 (6H, m, C4α, C9), 2.02- 1.95 (3H, dt, *J*=7.57, 4.60,C14), 1.86- 1.75 (12H, m, C23, C6β, C17), 1.75-1.70 (3H, m, C16α), 1.70- 1.57 (15H, m, C1α, β-$CH_{2\ dodecyl}$, C15β, C22α), 1.49- 1.41 (12H, m, C4β, C2β, C11), 1.41- 1.15 (72H, m, C6α, C8, C2α C16β, γ-CH_2, $(CH_2)_{8\ dodecyl}$, C20, C5), 1.11-1.04 (3H, m, C22β), 0.98- 0.91 (3H, m, C15α), 0.91 (9H, d, *J*=6.5, C21)), 0.88- 0.85 (9H, t, *J*=7.1, ω-$CH_{3\ dodecyl}$), 0.84 (3H, m, C1β), 0.82 (9H, s, C19), 0.59 (9H, s, C18).

Compound 6(M_w/ g mol^{-1}= 2537.99).^{13}C NMR (150 MHz, DMSO-d_6, 323 K) σ/ppm: 175.44 (C24), 71.01 (C12), 70.21 (C3), 66.16 (C7), 63.96 (α-$CH_{2\ dodecyl}$), 58.91 (NCH_2CH_2N), 50.19 (CH_3N), 49.46 (NCH_2CH_2N), 46.40 (C17), 45.60 (C13), 41.48 (C5), 41.15 (C14), 39.42 (C8), 39.38 (C4), 36.14 (C1), 35.52 (C20), 35.20 (C23), 34.75 (C10), 34.20 (C6), 32.93 (C22), 31.01 (β-$CH_{2\ dodecyl}$), 30.24 (C2), 28.79- 28.58 (γ-$CH_{2dodecyl}$, $(CH_2)_5$), 28.41 (C11), 28.37- 28.28 (CH_2), 27.16 (C16), 26.01 (C9), 25.69 (CH_2), 22.67 (C15), 22.32 (C19), 21.78 (CH_2), 21.67 (CH_2), 20.78 (CH_2), 17.23 (C21), 13.60 (ω- CH_3), 12.23 (C18).^{1}H NMR (600 MHz, DMSO-d_6, 50 °C) σ/ppm; 4.33 (4H, s br, OH-C3), 4.11 (4H, s br, OH-C12), 4.02 (4H, s br, OH-C7), 3.80-3.76 (4H, m, C12), 3.63-3.59 (4H, m, C7), 3.46-3.40 (12H, m, NCH_2CH_2N), 3.21-3.14 (4H, m, C3), 3.07 (12H, s, $(CH_3)_2$-N), 3.03 (6H, s, CH_3-N), 2.95-2.72 (8H, m, α-$CH_{2\ dodecyl}$), 2.26-2.19 (4H, q, *J*=12.9, C4α), 2.19- 2.11 (4H, dt, *J*= 4.76, C9),1.99- 1.93 (4H, dt, *J*=7.58, 4.5,C14), 1.84- 1.69 (20H, m, C23, C1α, C17, C16α), 1.69- 1.54 (20H, m, C15β, C6β, β-$CH_{2\ dodecyl}$, C22α), 1.46-1.39 (16H, m, C4β, C2β, C11), 1.38- 1.13 (96H, m, C6α, C8, C2α, γ-CH_2, $(CH_2)_{8\ dodecyl}$, C20, C5, C16β),1.07-1.00 (4H, m, C22β), 0.97- 0.89 (4H, m, C15α), 0.84-0.82 (4H, m, C1β), 0.88 (12H, d, *J*=6.6, C21),0.85 (12H, t, *J*=7.1, ω- $CH_{3\ dodecyl}$), 0.80 (12H, s, C19), 0.57 (12H, s, C18).

2.3. Measurements

Thermogravimetry, TGA, measured the loss of weight during heating with an instrument Shimatzu DTG-60H. Samples were heated from room temperature, RT to 573 K at the heating rate of 5 K min^{-1} in synthetic airflow of 50 mL min^{-1}. The temperature range for thermal analysis of the sample was determined by examination of TGA and DTA (*differential thermal analysis*) curves.

Differential scanning calorimetry, DSC, was carried out with a Perkin Elmer Pyris Diamond DSC calorimeter in N_2 atmosphere equipped with a model Perkin Elmer 2P intra-cooler, at the rate of 5 K min^{-1}. The transition enthalpy, Δ*H*/ kJ mol^{-1}, was determined from the peak area of the DSC thermogram; and the corresponding entropy change, Δ*S*/ J mol^{-1} K^{-1}, was calculated using the maximal transition temperature. All results are mean values of several independent measurements carried out on different samples of the same compound, taken from the first heating and cooling run.

Textures at room temperature were recorded by field emission scanning electron microscope FE-SEM, JEOL JSM-7000F. *Textures of heated samples* were examined with Leica DMLS polarized

optical light microscope, equipped with a Mettler FP 82 hot stage and Sony digital color video camera (SSC-DC58AP).

FTIR spectra were measured on an ABB Bomem MB102 spectrometer equipped with CsI optics and DTGS detector. Powders of **1, 3, 5** and **6** were recorded in transmission mode as pellets in KBr matrices with nominal resolution of 4 cm^{-1} and 10 scans both at room temperature and in temperature-dependent regime. Regarding the latter, Specac 3000 Series high stability temperature controller with heating jacket was used for the regulation of the heating rate, which was 5 K min^{-1}. Absorption IR spectra were taken every 5 K. Compound **1** was recorded from RT to 483 K, compound **3** from RT to 468 K, compound **5** from RT to 473 K and compound **6** from RT to 463 K. Compounds **2** and **4** were not recorded because of the simultaneous degradation or carbonization with melting that were detected with DSC and microscopy observations.

Diffraction patterns have been obtained by an automatic wide angle X-ray powder diffractometer, PXRD, Philips PW 3710, with monochromatized Cu Kα radiation (λ/ Å= 1.54056) and proportional counter, recorded at RT. The overall diffraction angle region was 2θ/ ^{o} = 3 – 60. The interlayer spacing (d_{hkl}) was calculated according to the Bragg's law.

3. Results and discussion

3.1. Room temperature measurements

Cholates shown on Scheme 1 are catanionic compounds formed by the anion-exchange reactions. Compounds differ in their cationic part, *i.e.* in the number of dodecyl chains on the same nitrogen atom in quaternary ammonium headgroups (**1** - **3**) and in the number of quaternary ammonium headgroups separated by ethylene spacers (**4** - **6**). The samples are identified with cation : anion ratio of 1 : 1 (**1** - **3**), 1 : 2 (**4**), 1 : 3 (**5**), 1 : 4 (**6**). Their structure is based on electrostatic interactions between negatively charged carboxyl oxygen from cholate (**1**, **2**, **4**–**6**) or carboxyl group from cholic acid (**3**), and positively charged nitrogen from quaternary ammonium headgroup.

All examined samples are characterized as layered structures at RT, seen as stacking of the layers with scanning electron microscopy images (Figure 1) and confirmed with PXRD measurements (Figure 2, Table S1 in the supplementary data). Picrates that have the same alkylammonium cations as examined cholates have also such arrangement, but with clearly distinguished hydrophobic and hydrophilic parts [4,32]. Moreover, results of dodecylpyridinium and *n*-alkyammonium cholates refer

to the smectic ordered phase at room temperature [23,27]. The bilayer like arrangement in the crystals of 1:1 *n*-alkyammonia cholate complexes contain *n*-alkyammonia guests included in the hydrophobic zones between the layers of cholate anions in a kind of sandwich-type structure [23]. According to these results, one can assume that the molecular arrangement of studied compounds resembles the previously mentioned one. The complex nature of steroidal compounds itself, and of their catanionic salts, makes the solving of the powder diffraction patterns tedious and hard. Due to strong affinity of such compounds to form very long but quite narrow needle-like crystals, it is also almost impossible to prepare satisfying monocrystals for X- ray diffraction, especially in the case of more complicated structures with the raising dodecyl chain or raising headgroup number in the molecule. Therefore, the complete structure determination of those compounds is still in progress, but they are qualitatively characterized in this work using IR spectroscopy.

Figure 1. Scanning electron microscopy images showing stacking of the layers for examined cholates: compounds **1** (**a**) and **6** (**b**). Bars are indicated.

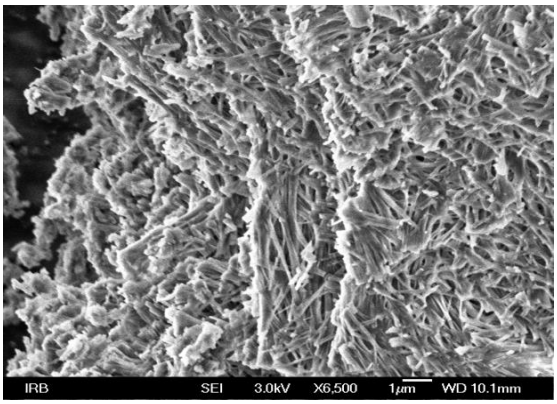

a

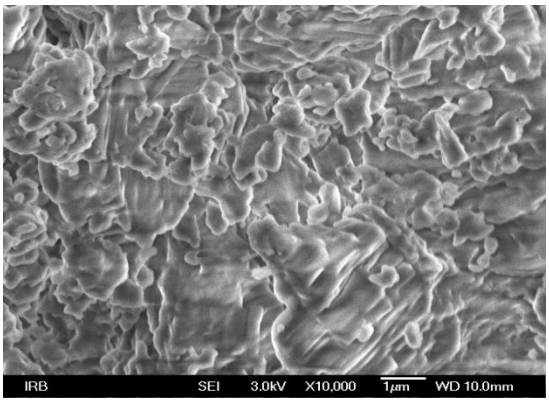

b

Figure 2. Wide angle X-ray scattering diffractograms of examined compounds **1** - **6** recorded at room temperature, indicating layered organization in the crystals.

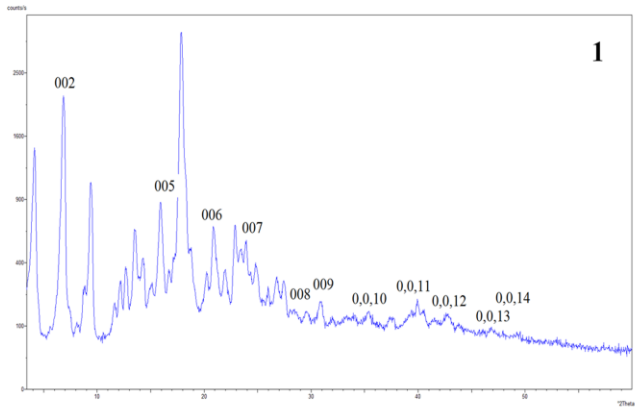

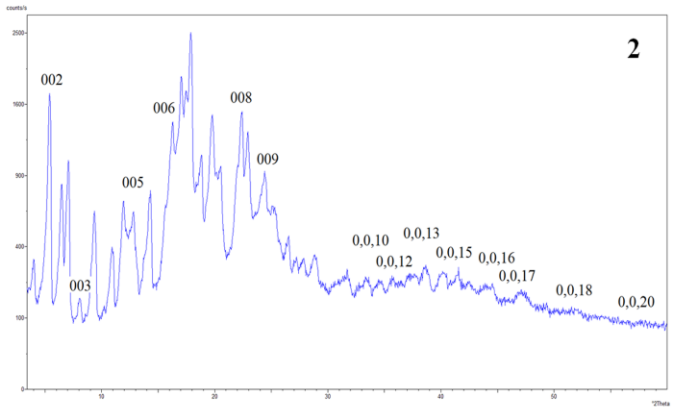

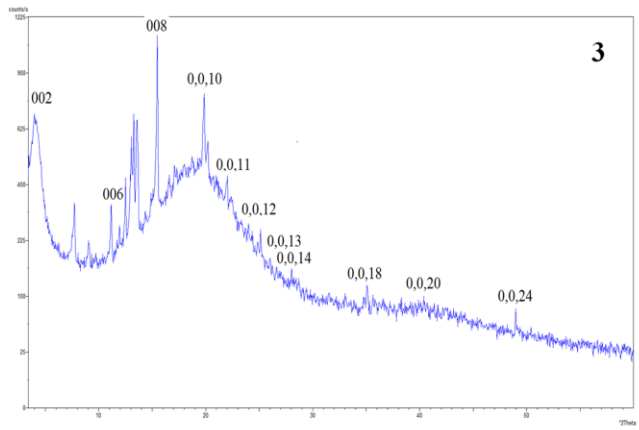

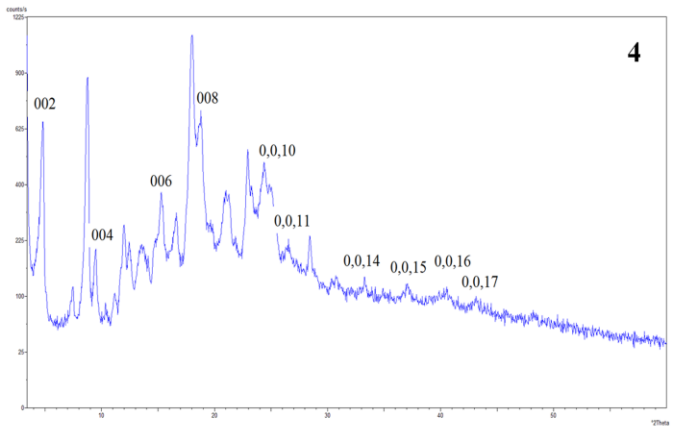

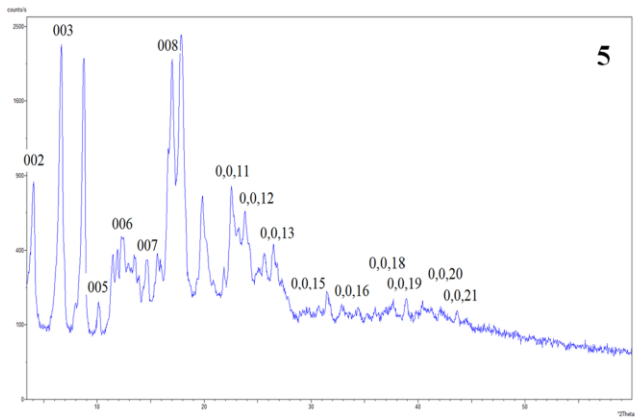

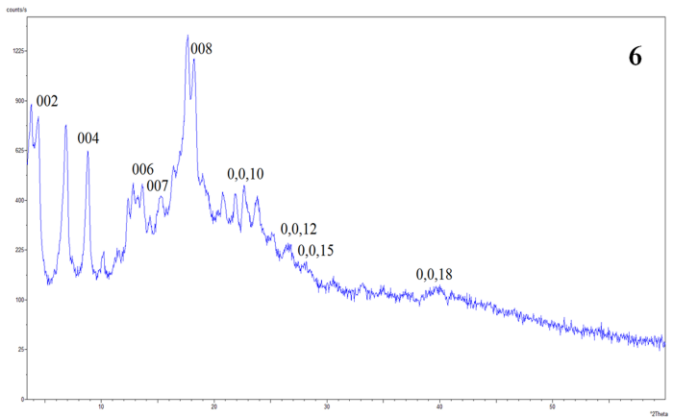

Table 1 presents assignation of infrared spectral bands of compounds **1**, **3**, **5** and **6** recorded as KBr pellets. Vibrations obtained at room temperature are roughly divided into two categories: the one originated from cholate moiety and the other due to long chain-moiety linked to the quaternary ammonium headgroup. The former ones are only partially assigned by Kolehmainen *et al.* [33] so more detailed description will be given here. The second ones, where some of the surfactants are described in our previous paper [32], will be elaborated here in more detail. Room temperature IR spectra of compounds **1**, **5** and **6** appear to be the same (Table 1, Figure 3), which is not unusual since they only differ in the number of alkyl chains and ammonium headgroups. IR spectrum of **3** (Table 1, Figure 3) is different than those previously mentioned since it was synthesized from different reactants. Strong and broad band in IR spectrum of **1**, **5** and **6** at 3359 cm^{-1} appears due to O-H stretching of cholate group, while the band attributed to the analogous normal mode in IR spectrum of **3** appears as medium strong broad band centered at about 3400 cm^{-1}. In addition, in IR spectrum of **1**, **5** and **6** a very weak band arise at 3036 cm^{-1} which may be due to the $=CH_2$ stretching of cholate moiety. As cholate group possess three hydroxyl groups, the one placed on C12 (Figure 3) can, together with methyl group on C13, exist in the form of keto-enol tautomer. Consequently, $=CH_2$ and C=C signals as well are to be expected. Signals at 2958 cm^{-1}, 2926 cm^{-1}, 2871 cm^{-1} and 2855 cm^{-1} in IR spectrum of **1**, **5** and **6** and at 2955 cm^{-1}, 2925 cm^{-1}, 2872 cm^{-1} and 2854 cm^{-1} in IR spectrum of **3** appear due to, respectively, asymmetric stretching of CH_3 group, asymmetric stretching of CH_2 group, symmetric stretching of CH_3 group and symmetric stretching of CH_2 group. As compound **3** is concerned, the absence of the broad feature between 3300 and 2500 cm^{-1}, usually attributed to the signals of COOH···COOH dimers, a common phenomenon for carboxyl acids, indicates that COOH group interacts with quaternary ammonium cation rather than with other COOH group. Medium strong and broad signal at 1740 cm^{-1} in IR spectrum of **3** is attributed to the C=O stretching of COOH moiety, as expected, since the compound **3** was the only one prepared from cholic acid. Compounds **1**, **5** and **6,** prepared from cholate anion, exhibit bands at 1560 cm^{-1} and 1399 cm^{-1} assigned as asymmetric and, respectively, symmetric stretching of COO^- group. In addition, in spectral region where usually double bonds generate signals, broad feature of different intensities appears in IR spectra of all compounds: at 1655 cm^{-1} (**1**, **5** and **6**) and at 1635 cm^{-1} (**3**). This absorption, attributed to the C=C stretching, goes along with the assumption on the existence of cholates in keto-enol form. Deformations of methylene group (CH_2) produce medium strong bands in IR spectrum of all compounds at 1467 cm^{-1}, while asymmetric and, respectively, symmetric deformation of methyl group (CH_3) appears at 1450 cm^{-1} and 1375 cm^{-1}. The stretching of carbon skeleton (-C-C-) is seen by medium strong and weak bands between1050 and 1090 cm^{-1} in IR spectra of **1**, **5** and **6** and, respectively, **3**. Vibrational motions that involve 4 atoms (rocking, wagging and twisting) of $C=CH_2$ moiety appear at 983 cm^{-1} and 645 cm^{-1} in IR spectra of **1**, **5** and **6**. The corresponding modes appear as weak and, respectively, very weak band at 982 cm^{-1} and 650 cm^{-1} in IR spectrum of **3**. The intensity relations in compounds **1**, **5** and **6,** when

compared with those in **3,** are in agreement with assumption that keto-enol equilibrium is more pronounced in **1**, **5** and **6** than in **3**. Deformations of CH_3 group below 1000 $cm^{-1}$are considered as insignificant for any discrimination between studied complexes, as well as the vibrations of hydrocarbon chains that contain more than four atoms in a row (about 724 cm^{-1} in IR spectra of all compounds) and, therefore, will not be further discussed.

Figure 3. Room temperature IR spectra of compounds **1**, **3**, **5** and **6**recoreded as KBr pellets. Abbreviations b.h. and a.h. indicate before and after heating, respectively.

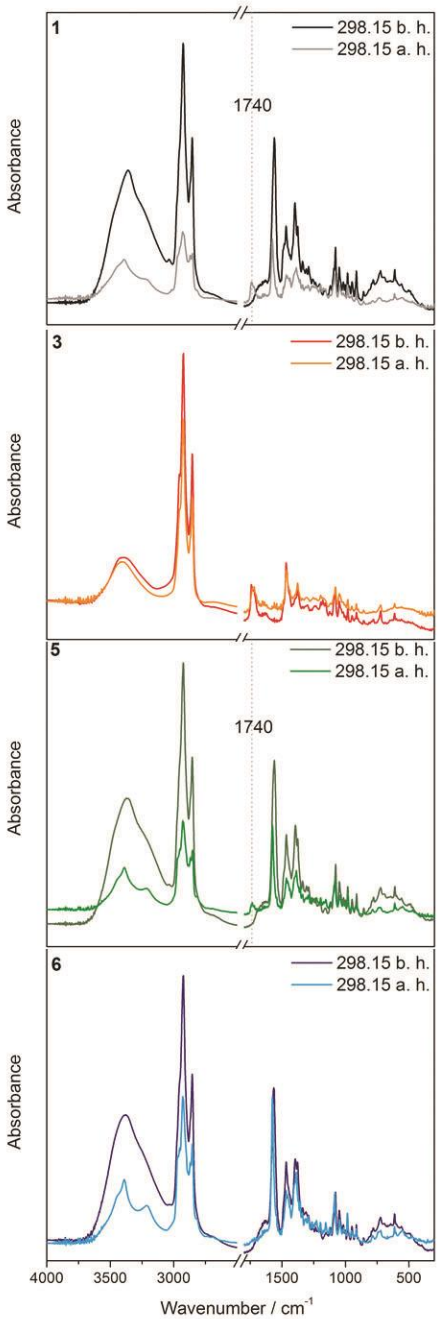

Table 1. IR spectra of compounds **1**, **3**, **5** and **6** recorded as KBr pellets. Band intensites are assigned as: vs-very strong, s-strong, m-medium, w-weak, vw-very weak, b-broad. Greek letters stand for: ν - stretching (ν_{as} for asymmetric, ν_{sym} for symmetric); δ - deformation; γ – wagging / rocking / twisting.

ν / cm^{-1}				
1	**3**	**5**	**6**	assignment
3359 s, b	3400 m, b	3359 s, b	3359 s, b	νO-H
3036 vw		3036 vw	3036 vw	ν $=CH_2$
2976 w		2976 w	2976 w	
2958 m	2955 m	2958 m	2958 m	$\nu_{as}CH_3$
2926 vs	2925 vs	2926 vs	2926 vs	$\nu_{as}CH_2$
2871 m	2872 m	2871 m	2871 m	$\nu_{sym}CH_3$
2855 s	2854 s	2855 s	2855 s	$\nu_{sym}CH_2$
2698 vw		2698 vw	2698 vw	
	1740 m, b			C=O (COOH)
1655 m, b	1635 w, b	1655 m, b	1655 m, b	C=C
1560 s		1560 s	1560 s	ν_{as} $(COO)^-$
1492 w	1490 vw	1492 w	1492 w	
1487 w		1487 w	1487 w	
1467 m	1467 m	1467 m	1467 m	δ CH_2
1450 vw		1450 vw	1450 vw	δ_{as} CH_3
1438 vw	1437 w	1438 vw	1438 vw	δ O-H
	1417 vw			
1399 m		1399 m	1399 m	ν_{sym} $(COO)^-$
	1397 w			
1375 m	1377 m	1375 m	1375 m	δ_{sym} CH_3
1338 w	1336 vw	1338 w	1338 w	
1324 vw		1324 vw	1324 vw	ν C-O $(COO)^-$
1309 w	1318 vw	1309 w	1309 w	
1290 w	1299 vw	1290 w	1290 w	ν C-N
	1272 vw			
1256 vw	1244 vw	1256 vw	1256 vw	
1236 vw	1232 vw	1236 vw	1236 vw	
1200 vw	1194 w	1200 vw	1200 vw	
1161 vw	1177 w	1161 vw	1161 vw	
	1156 w			
	1125 vw			
1118 w	1112 vw	1118 w	1118 w	
1090 m	1091 w	1090 m	1090 m	ν –C-C-
1078 m	1080 w	1078 m	1078 m	ν –C-C-
1049 m	1048 w	1049 m	1049 m	ν –C-C-
1036 w	1030 vw	1036 w	1036 w	
1017 w	1018 vw	1017 w	1017 w	
1001 w	1001 vw	1001 w	1001 w	
983 m	982 w	983 m	983 m	γ $C=CH_2$
969 w	946 w	969 w	969 w	
948 m		948 m	948 m	
924 w	924 vw	924 w	924 w	
913 m	913 w	913 m	913 m	γ CH_3
889 vw	901 vw	889 vw	889 vw	
858 w	854 vw	858 w	858 w	
816 vw	812 vw	816 vw	816 vw	
780 w	794 vw	780 w	780 w	γ CH_2
733 vw	780 vw	733 vw	733 vw	
729 vw		729 vw	729 vw	
724 w	723 w	724 w	724 w	-C-C-C-C-
693 vw	688 vw	693 vw	693 vw	
645 m, b	650 vw	645 m, b	645 m, b	γ $C=CH_2$
	632 vw			
613 w	613 w	613 w	613 w	
598 vw	580 vw, b	598 vw	598 vw	
558 w		558 w	558 w	
503 vw		503 vw	503 vw	
488 vw		488 vw	488 vw	

ν / cm^{-1}				
1	**3**	**5**	**6**	assignment
472 vw		472 vw	472 vw	
400 vw		400 vw	400 vw	
388 vw		388 vw	388 vw	
359 vw		359 vw	359 vw	
353 vw		353 vw	353 vw	
326 vw		326 vw	326 vw	

3.2. Temperature- dependent measurements

TGA and DTA analyses obtained the thermal stability of synthesized catanionics; compounds are stable until 473 K (**1**, **4** and **6**) and 483 K (**2**, **3** and **5**), when the great loss of mass occurs, indicating degradation or carbonization. Figure 4 and Table 2 show transition temperatures, *T*/ K, enthalpies, ΔH/ kJ mol^{-1}, and entropies, ΔS/ J mol^{-1} K^{-1}, during heating and cooling cycles, given by the DSC, and Figure 5 characteristic microphotographs of room and high temperature phases.

IR spectra of compounds that did not decompose (**1**, **3**, **5** and **6**) during thermal treatment were also recorded in the temperature-dependent regime (inserts in Figure 4). The spectra provide two very important informations; the structural changes of the sample, when heated, in qualitative terms, and the phase transition temperatures of the samples, reflected in the shift of the baseline absorption spectra [35]. The shift in baseline was monitored by measuring the absorbance at 2000 cm^{-1}, chosen because there is no absorption in IR spectrum of any sample at that wavenumber. Since the change of temperature normally induces the changes in vibrational spectra [36], here we will be focused only on those changes that can be regarded as relevant for explanation of thermal behavior of investigated compounds.

Figure 4. The thermograms obtained by differential scanning calorimetry for compounds **1** - **6** during heating (full lines), and cooling runs (dash-dot lines). The inserts show temperature-dependent changes in the baseline absorbance at 2000 cm^{-1}, obtained by infrared spectroscopy.

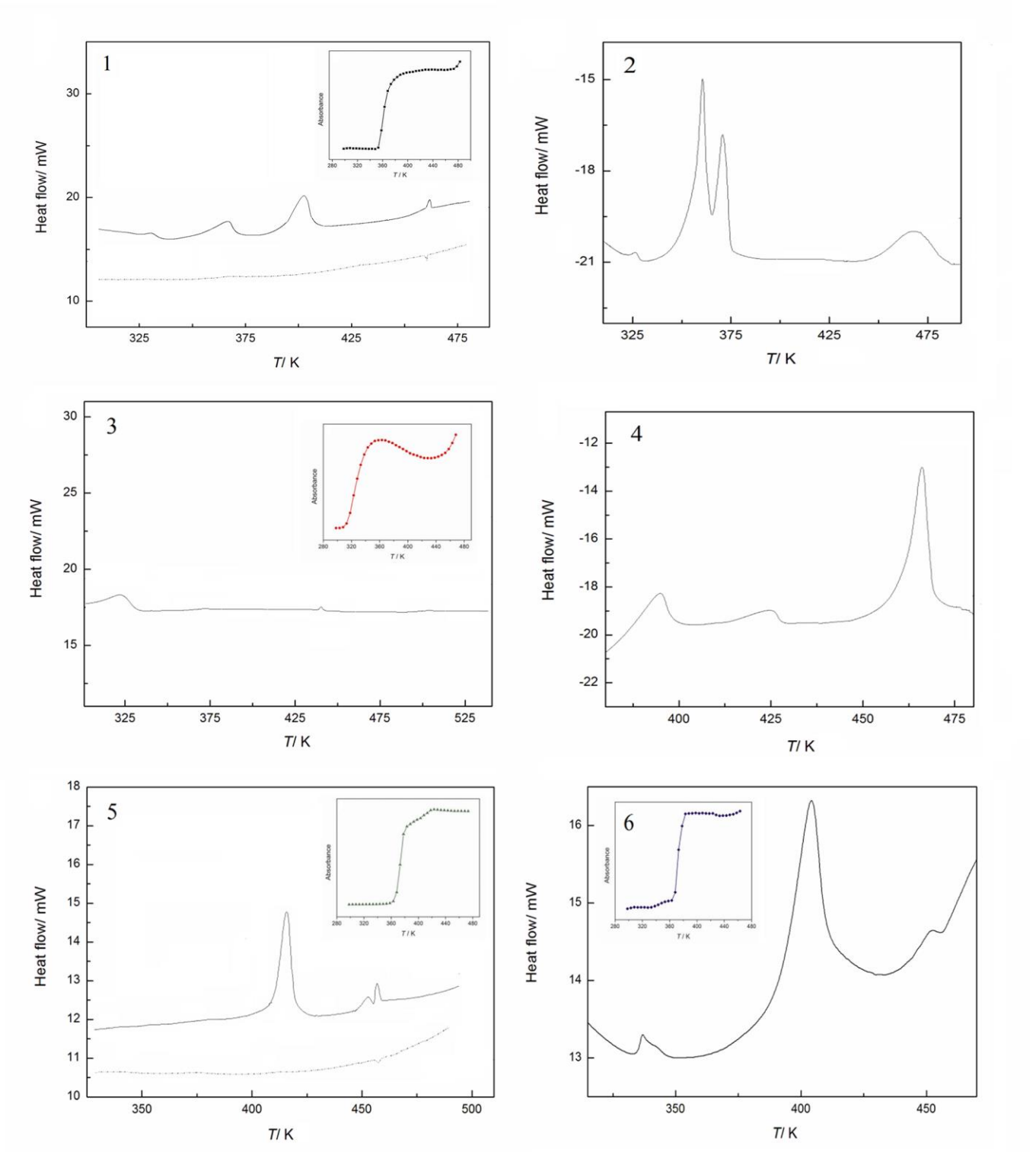

Table 2. Transition temperatures, T/ K, enthalpy changes, ΔH/ kJ mol^{-1}, and entropy changes, ΔS/ J mol^{-1} K^{-1} for studied cholates **1** - **6**.

Compound	Heating			Cooling		
	T/ K	ΔH/ kJmol^{-1}	ΔS/ JK^{-1}mol^{-1}	T/ K	ΔH/ kJmol^{-1}	ΔS/ JK^{-1}mol^{-1}
1	327 361 399 466	8.1 12.1 19.5 1.4	24.8 33.6 48.7 3.5	464**	-0.9	-2.0
2	325 361* 474	1.2 70.92 26.4	3.5 196.6 55.7	decomposition above 483 K		
3	320 444	12.53 0.03	39.10 0.07	slugged crystallization (24 h)		
4	395 425 470	26.4 5.6 54.2	66.9 13.2 112.9	decomposition above 473 K		
5	411 456 462	11.0 0.5 1.9	27.6 1.1 4.1	460**	-0.01	-0.06
6	336 404 453	4.1 47.3 2.3	12.2 117.2 5.1	slugged crystallization (72 h)		

*double peak

**complete crystallization after 48 h

The baseline shift in IR spectrum of **1** (Figure 4) suggests that phase transitions certainly occurs at 363 K. The temperature-dependent behavior of signals is addressed to the several most distinguished bands. First, there is O-H stretching, where one broad band centered at about 3359 cm^{-1} splits at temperatures above 363 K in two bands, the one at 3388 cm^{-1} and another at 3218 cm^{-1}. The band separation is getting greater with further heating (3403 cm^{-1} and 3226 cm^{-1} at 483 K) and the intensities are reduced. The band attributed to the asymmetric and, respectively, symmetric stretching of CH_3 group (2958 cm^{-1} and, respectively, 2871 cm^{-1}) increases in the whole temperature range and shifts to the lower wavenumbers (2951 cm^{-1} and, respectively, 2869 cm^{-1} at 483 K), where the most significant intensity gain appears at 363 K. The asymmetric and symmetric stretching of CH_2 group (2926 cm^{-1} and 2855 cm^{-1}) are somewhat different; the former increases with the temperature,

especially, at 363 K, and shifts to the higher wavenumbers (2930 cm^{-1} at 483 K), while the latter started to decrease when the temperature reached 393 K, suggesting that CH_2 stretching modes are more affected by the phase transition solid-liquid crystal. Medium strong broad feature at 1655 cm^{-1} decreases upon heating and vanishes above 363 K, indicating that keto-enol form of **1** is moved to the enol form cholate. Asymmetric stretching of COO^- moiety shifts to the higher wavenumbers and increases in intensity, especially when the system reaches the temperature of 363 K (from 1560 cm^{-1} to 1565 cm^{-1} for ν_{as}). In contrast, symmetric stretching decreases in intensity in shifts to the lower wavenumbers (from 1399 cm^{-1} to 1385 cm^{-1} for ν_{sym}). Skeletal vibrations at 1090 cm^{-1} and 1078 cm^{-1} increase with the temperature and merge at 363 K; further increase of the band is observed up to 393 K and then the band, with maximum at 1082 cm^{-1}, starts to decrease. Sample cooled down by standing on air for about one hour was again prepared as KBr pellet, and interestingly, the IR spectrum resembles more to the one recorded at 483 K than of 298 K, with the new band at 1740 cm^{-1}. This band is most likely attributed to the stretching of C=O group of cholates, implying that the heating and cooling the sample causes transition to keto form of cholate in compound **1**.

Unlike its bromide analogue, *i.e*. dodecyltrimethylammonium bromide, which undergoes only through one polymorphic transition before melting [37], compound **1** shows very rich thermal behavior. According to the DSC measurements, the transition at 361 K is attributed to the solid-solid phase transition, which is very close to the result obtained from IR measurements. When taking into account the IR results, at about 363 K the greatest changes are related to the stretching of COO^- moiety. Both symmetric and anitsymmetric stretching, as well as high-frequency shift of antisymmetric stretching of COO^- group may be related to the lower contribution of resonance stabilization with temperature. These changes occur simultaneously with the vanishing of the broad C=C stretching band and the change in the band shape of the OH stretching. The latter may overall suggest that bond lengthening in certain part of cholate moiety occurs and is accompanied by keto-enol balance within cholates, possibly comprising OH group bonded with C12, C13 and C18 segment. In effect, this may imply that, at this temperature, conformational changes within cholate moiety influence their ionic interaction with ammonium headgroup. Further temperature increment gives indications for certain phase transitions at 393 K and 483 K and they are, according to DSC, assigned as SmA mesophase formation (399 K) [38] and isotropisation (466 K). In IR spectra the corresponding transition is manifested through the shift of the absorption of the signals attributed to the stretching of CH_2 groups. Crystallization of compound **1** (Table 2) starts in forms of SmA [38] but this transition is very slow, and it takes 2 days (48 h) for this process to finish, resulting in focal conic SmC phase [38] (Figure 5a).

The introduction of the second alkyl chain (sample **2**) causes higher temperature of melting than of **1**, but with simultaneous degradation, followed by the complete decomposition above 474 K

(Table 2). The compound **2** also forms Maltese crosses at 324 K, typical for SmA phases [38]. It is also known that didodecyldimethylammonium bromide component exhibits a complex polymorphism through two liquid crystal phases on heating, of which the last one is identified as SmB phase, and a third phase appears on cooling [26]. To conclude, the thermotropic behavior of compound **2** is highly affected by cation and its thermal affinities. The double peak that occurs during thermal treatment can be the consequence of water evaporation and crystallization. Unfortunately, it was impossible to separate peaks by changing the heating rate of the sample, in order to analyze better these transitions.

According to its temperature-dependent IR spectra, sample **3** exhibits somewhat different behavior with the temperature increase when compared with compound **1**. The band at 3400 cm^{-1} gains intensity when heated up to 323 K, while at higher temperatures it decreases and absorbs at the same wavenumber. When compared with the analogous normal mode in compound **1**, the absence of splitting and band shift indicates that hydroxyl group is not so sensitive to the temperature in compound **3**. The band at 2954 cm^{-1} (asymmetric CH_3 stretching) remains at almost the same position in the whole temperature interval; its intensity increases and reaches a maximum at about 323 K, and remains approximately the same up to 373 K when it starts to decrease. The band at 2924 cm^{-1} (asymmetric CH_2 stretching) gains intensity above 323 K and, between 323 K and 373 K, it shifts to the higher wavenumbers (2926 cm^{-1}). At temperatures above 373 K the band intensity reduces, while its position remains unchanged. The band at 2872 cm^{-1} (symmetric CH_3 stretching) gains intensity up to 373 K; above that temperature, the band starts to decrease and absorbs at almost the same position. The similar behavior is observed for the band at 2854 cm^{-1} (symmetric CH_2 stretching) with one exception; the latter band reaches the maximum at 323 K and from this temperature and above it decreases. The medium strong and broad band originated due to C=O stretching gains intensity when heated, up to 373 K, while above this temperature it decreases. Additionally, the band becomes broader when increased in the whole temperature range (298 K- 468 K) and the high-frequency side asymmetry, observed at 298 K, disappears when the sample is heated up to 468 K. Above that temperature, the band becomes asymmetric on the low-frequency side. Skeletal vibrations in generally shift to the lower wavenumbers and decrease in intensity: 1091 cm^{-1} (298 K) shifts to 1087 cm^{-1} (468 K), 1079 cm^{-1} (298 K) shifts to 1076 cm^{-1} (468 K) and 1048 cm^{-1} (298 K) shifts to 1042 cm^{-1} (468 K). Qualitatively, before and after the heating the pellet, the sample **3** remains the same. Minor changes in the absorbance of the baseline at 2000 cm^{-1} (Figure 4) between 373 K and 443 K are followed by phase transition at 443 K.

Like its enantiotropic bromide analogue, *i.e.* tridodecylmethylammonium bromide [4], the viscous mass of compound **3** transforms into SmA phase [38], confirmed by the DSC (320 K, Figure 4, Table 2) and IR measurements (323 K, Figure 4). The peak at 444 K is defined as the one with very small values of enthalpy and entropy, characteristic for transition into isotropic liquid. Changes in the

positions of the bands attributed to the stretching of CH_2 groups are the most distinguished phenomena that occur at 323 K and 373 K, while interaction of COOH group with ammonium headgroup is not so sensitive to the temperature change, implying that all phase transtitions are related only with the reorganization of alkyl chains at mentioned temperatures. Crystallization after thermal treatment of the sample is kinetically managed, and seen as laces growing in some dendrite-like forms of SmC the next day [38] (Figure 5b).

Figure 5. Characteristic textures of examined cholates: focal conic textures of **1**, 48 hours after cooling to RT (**a**); smectic phase of compound **3**, 24 hours after cooling to RT (**b**); softening of the compound **5** crystals at 433 K, during heating cycle (**c**); and liquid crystals of **5** at 461 K, in cooling cycle (**d**). The bar corresponds to 250 μm.

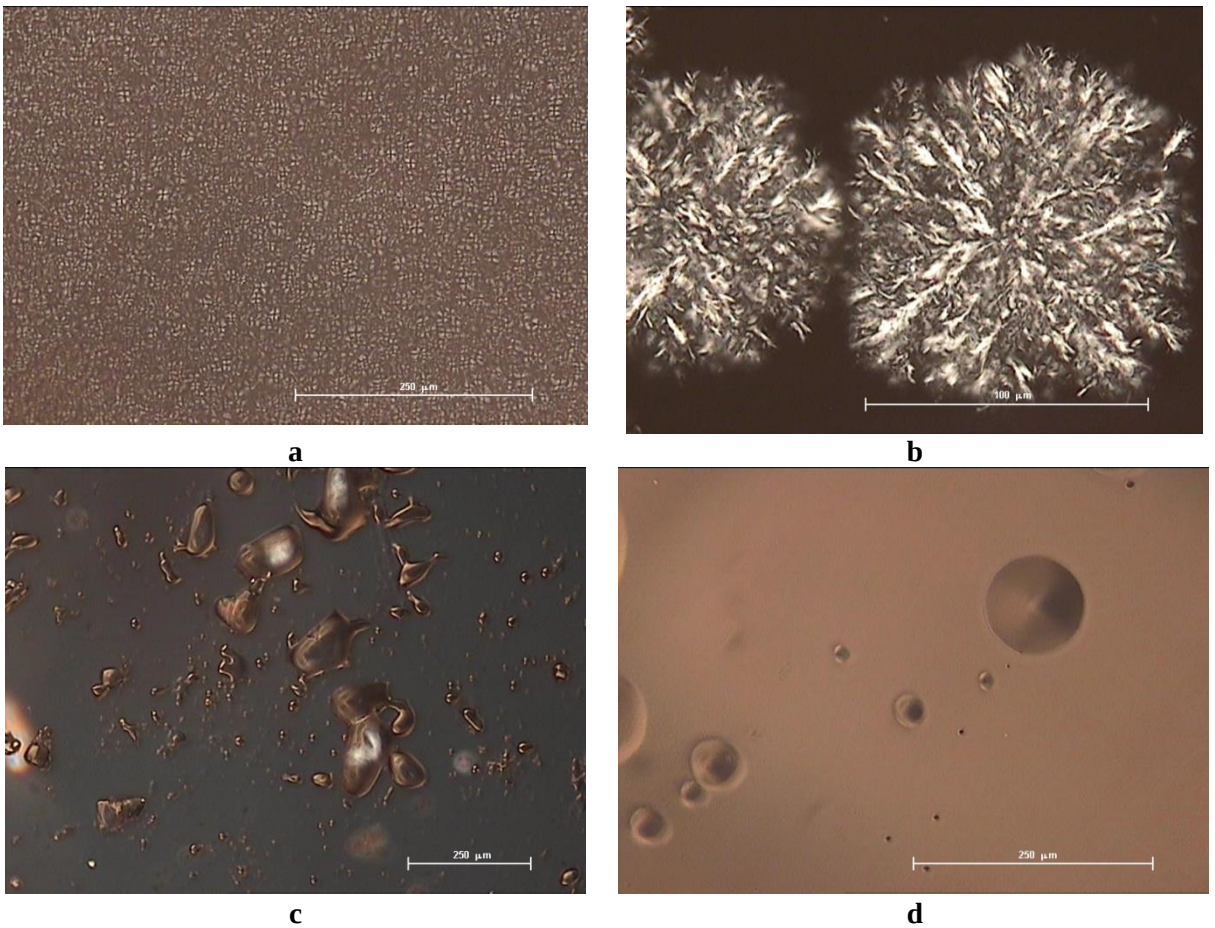

a **b**

c **d**

Previous studies on dimeric and oligomeric surfactant bromides, taken as the cationic components in synthesized catanionic cholates, obtained rich thermal behavior with molecules forming layers of Sm type with interdigitated *n*-dodecyl chains, lower ordering of solid phases and

diminishing mesophase stability with the higher degree of oligomerization [25]. Their cholate analogues **5** and **6** follow very similar behavior seen through polymorphism and LC formation. Unlike these compounds, the dimer dicholate (**4**) undergoes through crystal-crystal phase transitions until melting accompanied with carbonization at 470 K.

Due to their similarity, both in structural and in thermal-dependent terms, compounds **5** and **6** will be analyzed and interpreted together. First phase transition of compounds **5** and **6**, according to the absorbance value at 2000 cm^{-1} (Figure 4), occurs at 373 K for both compounds, and could point to polymorphic phase transition. The second transition (Figure 4) occurs at about 413 K (**5**) and, respectively, 423 K (**6**). Up to 473 K (**5**) and, respectively, 463 K (**6**), according to IR spectra, there are no phase transitions. Regarding temperature-dependent behavior of vibrational modes, we will discussed those related to the stretching of hydroxyl, methylene, methyl and carboxyl groups as well as the vibrations of skeleton. Strong and broad OH stretching band, centered at 3359 cm^{-1} at 298 K, suddenly gain intensity at 373 K in IR spectrum of both **5** and **6** compounds. As in the IR spectrum of **1**, this band splits into two bands with maxima at 3395 cm^{-1} and 3211 cm^{-1}. Above 413 K (**5**) and 423 K (**6**), the former gains intensity, while the latter remains the same. The band assigned as asymmetric CH_3 stretching shifts from 2958 cm^{-1} (298 K) to 2953 cm^{-1} (473 K in **5** and 463 K in **6**) in both **5** and **6** samples; its intensity increases when heated up to 413 K (**5**) and, respectively, 423 K (**6**). Asymmetric stretching of CH_2 group (2926 cm^{-1} at 298 K) increases up to 373 K and, at temperatures above that, its intensity reduces and the absorption shifts to 2930 cm^{-1} (473 K in **5** and 463 K in **6**). Symmetric stretching of CH_3 group, as well as the symmetric stretching of CH_2 group, produces the band that gains intensity up to 373 K. The former band starts to decrease above 413 K (**5**) and 423 K (**6**) and absorbs at 2869 cm^{-1}, while the latter remains of more or less the same intensity and absorbs at the 2956 cm^{-1} (up to 473 K (**5**) and, respectively, 463 K (**6**)). According to the observed temperature-dependent behavior, both CH_3 and CH_2 group are affected by the polymorphic phase transitions that occurred for both compounds **5** and **6**. Medium broad feature at 1655 cm^{-1} decreases with temperature and vanishes above 373 K in both **5** and **6** compounds, implying that the keto-enol equilibrium is shifted to the enol side. Asymmetric stretching of COO^- group (1590 cm^{-1} at 298 K in both **5** and **6**) continuously moves to the higher frequencies and gains intensity, especially at 373 K. The increase in intensity is observed up to 413 K (**5**) and 423 K (**6**) when it starts to decrease. At 473 K (**5**) it absorbs at 1565 cm^{-1} and, respectively, at 463K (**6**) at 1570 cm^{-1}. Symmetric stretching of COO^- group (1399 cm^{-1} at 298 K in IR spectra of both **5** and **6**) shifts to the lower wavenumbers and, at 373 K, suddenly increases in intensity. At 473 K (**5**) and 463 K (**6**) the band appears at 1385 cm^{-1} in both complexes. The bands at 1090 cm^{-1} and 1078 cm^{-1}, attributed to the stretching of -C-C- moiety, increase with the temperature and merge at 373 K. Above 413 K in IR spectrum of compound **5** and at 423 K for compound **6** the observed asymmetric band reduces in intensity. The band at 1049 cm^{-1} gradually moves to the lower frequencies in both samples and decrease in intensity (1042 cm^{-1} at 473 K (**5**) and

463 K (**6**)). After accomplishing the temperature of 473 K (**5**) and 463 K (**6**), the samples were cooled down to the RT, by standing on air for about one hour and prepared again as KBr pellet. Similarly as for compound **1**, spectra of **5** and **6** resemble more to the IR spectra at 473 K (**5**) and 463 K (**6**) than the one recorded at 298 K. A major exception is the appearance of the new band at 1740 cm^{-1} in **5**, as seen for **1** also, and is attributed to the stretching of C=O group of cholate moiety present in keto-form. In compound **6**, interestingly, this band is not observed, suggesting, therefore, that the sample remains the same after the heating and cooling.

Polymorphic phase transitions are changes at the structural level, very often not detected by DSC and microscopy observations, but with IR measurements. According to that, most of the solid-solid phase transitions, this means the structural changes of compounds **5** and **6** seen with the IR measurements at 373 K are not registered with the DSC or microscopy. The exception is the leaf-like textures formation in compound **6** at 336 K, explained with the same phenomena. The conformation changes within cholate moiety occur at the same temperature (373 K in both **5** and **6**) at which the absorbance of the band attributed to the antisymmetric stretching of COO^- group(s) rapidly gains intensity. From the perspective of structural changes at 373 K, it is very likely that conformational changes precede the change in ionic interaction of COO^- group(s) with ammonium headgroup. The most drastic changes in the signals originated from COO^- moieties, due to its interaction with ammonium headgroup, appear between 413 K and 473 K (IR) in **5** and, respectively, 423 K and 463 K (IR) in **6**. For compound **5**, the phase transition at 411 K in DSC (413 K in IR) is, according to the microscopic observations, attributed to the softening of the crystal (Figure 5c, Table 2) that occurs during thermal treatment of compound **5** as the process before LC formation (456 K in DSC). Compound **6** undergoes LC phase formation at 404 K with respect to DSC (423 K in IR), as seen in Table 2 and Figure 4. This transition is seen through formation of slightly striated conic textures typical for SmA [38]. After that, both compounds undergo through the processes of isotropic liquid formation registered at 461 K (DSC) and at 473 K (IR) for compound **5** and at 453 K (DSC) and 463 K (IR) for **6**. Aside the changes in ionic interactions the isotropisation is manifested as well through changes in vibrations of CH_2 groups. Crystallization of compound **5** in forms of SmA cones [38] (Figure 5d) starts immediately after isotropisation, when sample is cooled to RT. The crystallization of compound **6** is slugged, and finishes three days (72 h) after cooling the sample to RT as SmC smooth focal conic textures [38].

Figure 6. The dependence of isotropisation temperatures (T/ K), enthalpy (ΔH/ kJ mol^{-1}) and entropy changes (ΔS/ J mol^{-1} K^{-1}) in the heating cycle versus: (**a**) the total number of dodecyl chains in the molecule, n_c = 1 - 3, for compounds **1** - **3**; (**b**) the ascending ammonium headgroup number, n_h = 2 - 4, for compounds **4** - **6**.

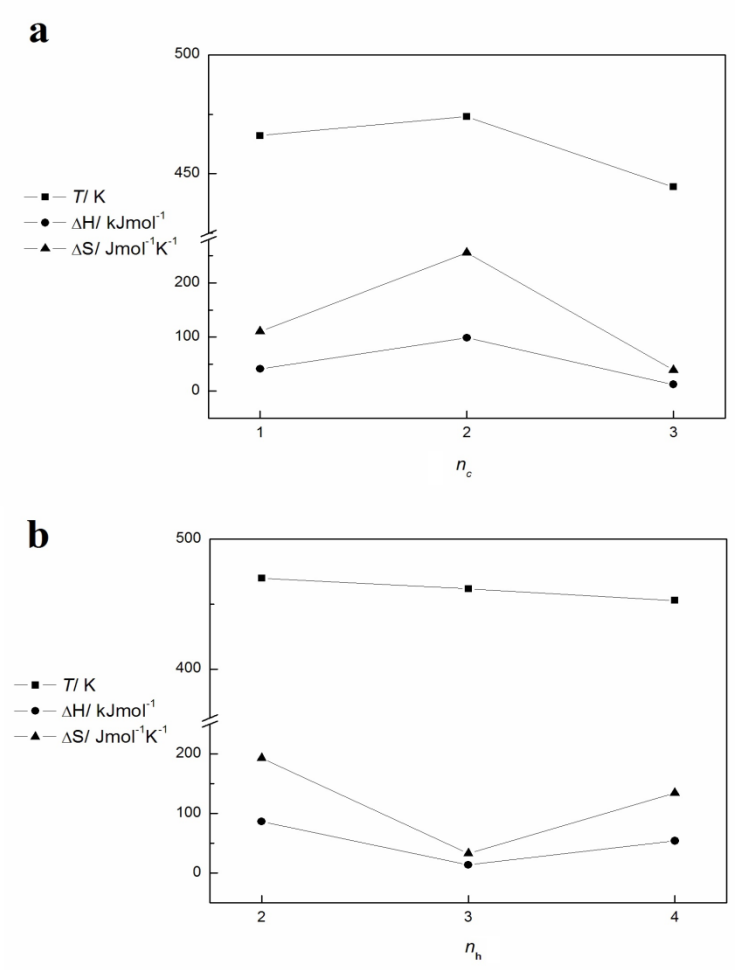

In summary, according to the observed temperature-dependent behavior in IR spectra of compounds **1**, **5** and **6**, the most drastic spectral changes are associated with the COO^- group and its interaction with quaternary ammonium headgroups. Changes in methyl and methylene vibrations can be considered as second order effects, when compared to the former ones. It seems that informations obtained from DSC measurements and baseline shifts from IR spectra, when the structural changes in the sample associated with carbon chains are concerned, coincide within 10 %.

The temperature of isotropisation and thermodynamic parameters of overall phase transitions for compounds **1** (n_c = 1), **2** (n_c = 2) and **3** (n_c = 3) follow polynomial regression (Figure 6a) with the total number of *n*-dodecyl chains in the molecule, n_c = 1 – 3:

$$T/\text{ K} = 480.54 + 64.24\, n_c - 18.76\, n_c^2 \quad (1)$$

$$\Delta H \text{ kJ mol}^{-1} = -159.70 + 272.49\, n_c - 71.69\, n_c^2 \quad (2), \text{ and}$$

$$\Delta S/\text{ J K}^{-1}\text{ mol}^{-1} = -396.43 + 687.95\, n_c - 180.92\, n_c^2 \quad (3);$$

with the maximum values for compound **2**, as expected, because of the previously mentioned melting and the beggining of degradation, that in general show large enthalpy and entropy values.

The lower enthalpy and entropy changes for phase transitions of compounds **1** and **3** indicate greater ordering of the structures with one and particularly with three dodecyl chains in the molecule, in contrast to the structures with even (two) number of chains (compound **2**). The crystallization period of the isotropic melt also contributes this fact. The process of crystallization for compound **1** starts immediately when cooling from the isotropic liquid, but it takes much more time to complete (48 h) than that of compound **3** (24 h), which can be explained due to three additional trimethyl chains that seriously affect the rate of structure arrangement solidification of **1**. That kind of difficulties in recovering the original state from the disordered state, associated with slugged crystallization is well known [37].

In contrast to the catanionic compound **1**, whose simple bromide analogue is thermally more stable [37], compounds **2** and **3** are more stable than related bromides [4, 26], while previously studied picrate analogues show linear dependence of temperature and thermodynamic phase transition parameters [4]. This differenence can be explained by the structural (nonplanar structure of cholate molecule and planar, resonance stabilized structure of picrate molecule) and geometric factors (the interplay of ionic and hydrocarbon layers) that greatly affect their molecular packing and consequently their thermal behavior.

The more complex architecture of oligomeric cationic surfactant makes the crystallization process of examined catanionic complexes (samples **4** – **6**) more complicated and slower (Figure 4, Table 2). The steric hindrance factors cause harder pairing of charges and slugged formation of crystal lattice, which can be seen during somewhat difficult solid phase formation after isotropization on cooling. The dimeric dicholate (**4**, $n_h = 2$) is the less complex structure in this group, but obviously less stable during heating treatment, seen through tendency to degradate. Surprisingly, the growing complexity in oligomeric cholates provides formation of thermally more stable compounds with expressed enantiotropic properties. The progressive slugged crystallization of the samples **5** (48 h, $n_h = 3$, Table 2) and **6** (72 h, $n_h = 4$, Table 2) that lasts in days, as well as observed increase of structure disorder (Figure 6b) is the result of more and more complex structures. If we take into account that this phenomenon is common for polymers, then we could say that it was expected to happen. The structure of tetramer tetracholate (**6**) is very close to what is called polymeric structure, so this property prevails among all other physico-chemical tendencies.

Catanionic compounds **4 - 6** have lower isotropisation temperatures than related bromides, and unlike trimer tribromide [25], the cholate analogue does not decompose during this process. Considering the thermodynamic parameters of oligomeric cholates (Figure 6b), unlike for picrate and bromide analogues that follow linear growth [25,32], the ascending ammonium headgroup number n_h leads to the lower values of isotropisation temperatures (T/ K), following linear equation:

$$T/\,\mathrm{K} = 487.34 - 8.59\, n_h \qquad (4).$$

The descending enthalpy and entropy changes follow the polynomial equations (5) and (6):

$$\Delta H/\ \text{kJ mol}^{-1} = 571.1 - 355.55.n_h + 56.55\ n_h^2 \quad (5)\ \text{and}$$

$$\Delta S/\ \text{J K}^{-1}\,\text{mol}^{-1} = 1299.1 - 814.95\ n_h + 130.95\ n_h^2 \quad (6),$$

and the resulted dependence can, again be explained with flourishing polymeric character of the samples. The thermal properties of oligomeric cholates **4** – **6** indicate more compositive chemical structure, but also specific thermodynamic stability trend owing advanced polymer-like structure.

Unlike for studied compounds, thermotropic mesomorphism was not detected for dioctyldimethylammonium and dinonyldimethylammonium cholate, and their temperatures of isotropisation are far lower [33]. On the other hand, poly(oxyethylene) cholesterol ethers with shorter oxyethylene chain or less than ten oxyethylene units (that is less than twenty carbon atoms) exhibit liquid crystalline (LC) properties [34]. This is in accordance with the well-known fact that LC properties of quaternary ammonium salts improve along with the chain length [2,30,33]. Moreover, the dodecylpyridinium group does not promote thermotropic mesomorphism, causes thermally less stable catanionic cholate [27] than studied alkylammonium cholates, as the consequence of the positive charge delocalized over the whole cationic aromatic pyridinium system that weakens cation/anion electrostatic interactions between components [39]. These examples clearly point to the dominance of quaternary ammonium part in examined cholates. Moreover, thermogravimetric and microscopic analysis of sodium cholate (cholic acid) reveals melting as the only phase transition at *cca.* 443(458) K accompanied with decomposition until 954(730) K. The results of Shopova and Milkova for cholic acid are quite similar with minor variations in temperature; the decomposition process occurs in the period 473-693 K, during which the steroidal skeleton completely collapses at 658 K [40]. The previously made comparison of synthesized cholates with thermal behavior of their cationic components, *i.e.* bromide analogues [4,25,26,37], and the provided results doubtlessly point to the dominant role of quaternary ammonium centers (cationic surfactant). The dominance of cationic surfactant variation is seen through rich thermal behavior of catanionic cholates, diversity in phase transitions of each examined cholate ; polymorphism, slugged crystallization, simultaneous melting and decomposition, and high affinity to form LC phases. These properties depend partly on their own, and partly on the whole catanionic structure, as well as on the geometric factors and molecular packing in the interplay of ionic and hydrocarbon layers. Polymorphic transitions originate mostly from structural and conformational changes in the alkyl chains of the cationic part, because it is less unlikely that the rigid steroid skeleton rearranges its conformation easily [33]. Moreover, as the Coulomb interactions in the ionic layer are much stronger than van der Waals forces in the

hydrocarbon layers, the ionic layers stay unchanged by heating, with conformational or positional disorder at lower temperatures causing polymorphic phase transitions, and formation of LC phases.

4. Conclusions

The novel catanionic compounds based on cholate anion synthesized in equimolar solutions of components were identified by NMR spectroscopy. Thermogravimetry and differential thermal analysis, microscopy, differential scanning calorimetry, IR spectroscopy, and PXRD measurements were used complementary in order to obtain their structural and physico-chemical, in particular thermotropic properties. Cholate complexes are divided into two groups; the ones with the growing number of alkyl chains attached on the same headgroup in the cationic part (compounds **1** – **3**), and the ones with increasing number of ammonium headgroups connected by an ethylene spacers (**4** – **6**). The examined samples are characterized at RT as layered structures, crystal smectic phases, confirmed with PXRD measurements and seen as stacking of the layers with scanning electron microscopy. Their thermal behavior is function of their structure, seen through polymorphism in the crystalline state, and smectic mesophase formation; melting with simultaneous degradation or prompt carbonization; kinetically managed crystallization in forms of dendrite-like or focal conic textures. Temperature changes of IR spectra indicate the movement of the cholates keto-enol isomer balance, resulting with the prevalence of the enol form in the sample **3,** and keto form in samples **1** and **5** after thermal treatment and cooling, while sample **6** remains the same before and after heating. Temperatures of isotropisation follow polynomial regression with the total number of dodecyl chains in the molecule, linear descending trend for compounds with increasing number of ammonium headgroups, and are far higher than of related picrate analogues indicating thermally more stable alkylammonium cholates. The thermal behavior and thermodynamic parameters of oligomeric cholates of more compositive chemical structure, indicate advanced trend of polymer-like structures. The obtained results demonstrate the easy way of controlling the properties of new compounds by changing one part of the molecule, and as the result making new materials with well-planned physico-chemical properties.

Acknowledgments. This work has received support from the Ministry of Education, Science and Sport of the Republic of Croatia (Project Nos 098-0982915-2949 and 098-0982904-2927). We are grateful to dr. sc. J. Makarević, Department of Organic Chemistry and Biochemistry, Ruđer Bošković Institute, Zagreb, for the help with the NMR spectra.

References

[1] N. Kimizuka, Self-assembly in mesoscopic dimension and artificial supramolecular membranes, Curr. Opin. Chem. Biol. 7 (2003) 702–709.

[2] T. Kunitake, Synthetic Bilayer Membranes: Molecular Design, Self-Organization, and Application, Angew. Chem. Int. Ed. Engl. 31 (1992) 709–726.

[3] J.-H. Fuhrhop, J. Köning, Membranes and molecular assemblies the synkinetic approach, Royal Society of Chemistry, Cambridge, 1994.

[4] T. Mihelj, Z. Štefanić, V. Tomašić, Thermal and structural properties of surfactant–picrate compounds, J. Therm. Anal. Calorim. 108 (2012) 1261–1272.

[5] T. Mihelj, V. Tomašić, Amphiphilic Properties of Dodecylammonium Chloride/4-(1-Pentylheptyl) Benzene Sodium Sulfonate Aqueous Mixtures and Study of the Catanionic Complex, J. Surfactants Deterg. 17 (2014) (2) 309-321.

[6] V. Tomašić, N. Filipović-Vinceković, B. Kojić-Prodić, N. Kallay, Precipitation and association in a mixture of dodecylammonium chloride and sodium dodecyl sulfate in aqueous medium, Colloid Polym. Sci. 269 (1991) 1289–1294.

[7] M. Vinceković, D. Jurašin, V. Tomašić, M. Bujan, N. Filipović-Vinceković, Interactions in Aqueous Mixtures of Alkylammonium Chlorides and Sodium Cholate, J. Dispers. Sci. Technol. 27 (2006) 1099–1111.

[8] N. Filipović-Vinceković, D. Škrtić, V. TomaŠić, Interactions in Dodecylammonium Chloride/Dodecyl Sulfate Systems, Beri Bunsen Ges Phys Chem. 95 (1991) 1646–1651.

[9] A.F. Hofmann, Bile acids as drugs: principles, mechanisms of action and formulations, Ital. J. Gastroenterol. 27 (1995) 106–113.

[10] F. Berlati, G. Ceschel,, C. Clerici,, R. Pellicciari, A. Roda, C. Ronchi, The use of bile acids as antiviral agents, WO 9400126 1994, n.d.

[11] B. Marples, R. Stretton, Use of steroidal compounds as anti-fungal agents, WO 9013298, n.d.

[12] P.B. Savage, C. Li, U. Taotafa, B. Ding, Q. Guan, Antibacterial properties of cationic steroid antibiotics, FEMS Microbiol Lett. 217 (2002) 1–7.

[13] A.P. Davis, J.-B. Joos, Steroids as organising elements in anion receptors, Coord Chem Rev. 240 (2003) 143–56.

[14] S. Nath, U. Maitra, A Simple and General Strategy for the Design of Fluorescent Cation Sensor Beads, Org Lett. 8 (2006) 3239–42.

[15] V.H. Soto Tellini, A. Jover, F. Meijide, J. Vázquez Tato, L. Galantini, N.V. Pavel, Supramolecular Structures Generated by a p-tert-Butylphenyl-amide Derivative of Cholic Acid: From Vesicles to Molecular Tubes, Advan Mater. 19 (2007) 1752–6.

[16] M. Yoshii, M. Yamamura, A. Satake, Y. Kobuke, Supramolecular ion channels from a transmembrane bischolic acid derivative showing two discrete conductances, Org Biomol Chem. 2 (2004) 2619–23.

[17] L.W. Judd, A.P. Davis, From cholapod to cholaphane transmembrane anion carriers: accelerated transport through binding site enclosure, Chem Comm. 46 (2010) 2227–9.

[18] R.P. Bonar-Law, L.G. Mackay, J.K.M. Sanders, Morphine recognition by a porphyrin–cyclocholate molecular bowl, J Chem Soc Chem Commun. (1993) 456–8.

[19] R. Balasubramanian, U. Maitra, Design and Synthesis of Novel Chiral Dendritic Species Derived from Bile Acids, J Org Chem. 66 (2001) 3035–3040. doi:10.1021/jo0013305.

[20] U. Maitra, S. Balasubramanian, Design and synthesis of new bile acid-based macrocycles, J. Chem. Soc. [Perkin 1]. (1995) 83–88.
[21] K. Kato, N. Tohnai, M. Miyata, Hierarchical Prediction Process of Cholic Acid Crystal Structures Based on Characteristic Helical Assemblies, Mol. Cryst. Liq. Cryst. 440 (2005) 125–132.
[22] M. Miyata, K. Sada, Deoxycholic Acid and Related Hosts, in: J.L. Atwood, J. Davies, D. McNicol, J. Lehn, F. Toda, R. Bishop (Eds.), Compr. Supramol. Chem., Pergamon, Oxford, 1966: pp. 147–176.
[23] V. Tomašić, Z. Štefanić, Cholic acid as host for long linear molecules: a series of co-crystals with n-alkylammonia, Cryst. Eng. Comm. 9 (2007) 1124–8.
[24] N. Filipovic-Vincekovic, V. Tomasic, Solid-State Transitions of Surfactant Crystals, in: N. Garti (Ed.), Therm. Behav. Dispersed Syst., CRC Press, 2000: pp. 451– 476.
[25] D. Jurašin, A. Pustak, I. Habuš, I. Šmit, N. Filipović-Vinceković, Polymorphism and Mesomorphism of Oligomeric Surfactants: Effect of the Degree of Oligomerization, Langmuir. 27 (2011) 14118–14130.
[26] M. Godlewska, S. Wróbel, B. Borzęcka-Prokop, M. Michalec, P. Dynarowicz, Phase Behavior of Didodecyldimethylammonium Bromide, Mol. Cryst. Liq. Cryst. Sci. Technol. Sect. Mol. Cryst. Liq. Cryst. 300 (1997) 113–126.
[27] T. Mihelj, V. Tomašić, Thermal Behavior of Dodecylpyridinium Based Surfactant Salts with Varied Anionic Constituent, J. Dispers. Sci. Technol. doi:10.1080/01932691.2013.811683.
[28] B.F.B. Silva, E.F. Marques, Thermotropic behavior of asymmetric chain length catanionic surfactants: The influence of the polar head group, J. Colloid Interface Sci. 290 (2005) 267–274.
[29] I. Stella, A. Müller, Mesomorphic behaviour of N-(n-alkyl) pyridinium hydrogensulfates, Colloids Surf. Physicochem. Eng. Asp. 147 (1999) 371–374.
[30] V. Tomasic, S. Popovic, N. Filipovic-Vincekovic, Solid State Transitions of Asymmetric Catanionic Surfactants, J. Colloid Interface Sci. 215 (1999) 280–289.
[31] V. Tomašić, S. Popović, L. Tušek-Božić, I. Pucić, N. Filipović-Vinceković, A novel catanionic surfactant: Hexadecyltrimethylammonium dodecyl sulfate, Berichte Bunsenges. Für Phys. Chem. 101 (1997) 1942–1948.
[32] V. Tomašić, N. Biliškov, T. Mihelj, Z. Štefanić, Thermal behaviour and structural properties of surfactant—Picrate compounds: The effect of the ammonium headgroup number, Thermochim. Acta. 569 (2013) 25–35.
[33] E. Kolehmainen, M. Lahtinen, A. Valkonen, B. Behera, R. Kauppinen, N,N-Di-n-octyl-N,N-dimethyl and N,N-di-n-nonyl-N,N-dimethyl ammonium cholates: 13C and 15N CPMAS NMR, powder X-ray diffraction and thermoanalytical characterization, J. Mol. Struct. 930 (2009) 201–208.
[34] M.A. López-Quintela, A. Akahane, C. Rodrıguez, H. Kunieda, Thermotropic Behavior of Poly(oxyethylene) Cholesterol Ethers, J. Colloid Interface Sci. 247 (2002) 186–192.
[35] B. Zimmermann, G. Baranović, Determination of phase transition temperatures by the analysis of baseline variations in transmittance infrared spectroscopy, Appl. Spectrosc. 63 (2009) 1152–1161.
[36] K.H. Illinger, D.E. Freeman, Temperature dependence of infrared and Raman intensities, J. Mol. Spectrosc. 9 (1962) 191–203.
[37] K. Iwamoto, Y. Ohnuki, K. Sawada, M. Senō, Solid-Solid Phase Transitions of Long-Chain n-Alkyltrimethylammonium Halides, Mol. Cryst. Liq. Cryst. 73 (1981) 95–103.
[38] G.W. Gray, J.W. Goodby, Smectic Liquid Crystals - Textures and Structures, Leonard Hill, Glasgow and London, 1984.
[39] S. Misaki, S. Takamatsu, M. Suefuji, T. Mitote, M. Matsumura, The Synthesis of Fluorine Containing Phenyl Benzoates and Their Properties as Liquid Crystals, Mol. Cryst. Liq. Cryst. 66 (1981) 123–132.
[40] N. Shopova, T. Milkova, Thermochemical decomposition of cholic acid and its derivatives, Thermochim. Acta. 255 (1995) 211–220.